The Meteoritical Society

Meteoritics & Planetary Science 55, Nr 3, 558–574 (2020)
doi: 10.1111/maps.13453

The brecciated texture of polymict eucrites: Petrographic investigations of unequilibrated meteorites from the Antarctic Yamato collection

Christian VOLLMER[1*], Stella ROMBECK[1], Julia ROSZJAR[2], Adam R. SARAFIAN[3], and Stephan KLEMME[1]

[1]Institut für Mineralogie, Westfälische Wilhelms-Universität Münster, Corrensstrasse 24, D-48149 Münster, Germany
[2]Department of Mineralogy and Petrography, Natural History Museum Vienna, Burgring 7, 1010 Vienna, Austria
[3]Science and Technology Division, Corning Incorporated, 21 Lynn Morse Rd., Painted Post, New York, New York 14870, USA
[*]Corresponding author. E-mail: christian.vollmer@wwu.de

(Received 29 January 2019; revision accepted 24 January 2020)

Abstract–We report on the petrography and mineralogy of five Yamato polymict eucrites to better constrain the formation and alteration of crustal material on differentiated asteroids. Each sample consists of different lithic clasts that altogether form four dominant textures and therefore appear to originate from closely related petrological areas within Vesta′s crust. The textures range from subophitic to brecciated, porphyritic, and quench-textured, that differ from section to section. Comparison with literature data for these samples is therefore difficult, which stresses that polymict eucrites are extremely complex in their petrography and investigation of only one thick section may not be representative for the host rock. We also show that sample Y-793548 consists of more than one lithic unit and must therefore be classified as polymict instead of monomict. The variety and nature of lithic textures in the investigated Yamato meteorites indicate shock events, intense post-magmatic thermal annealing, and secondary alteration. These postmagmatic features occur in different intensities, varying from clast to clast or among coexisting mineral fragments on a small, local scale. Several clasts within the eucrites studied have been modified by late-stage alteration processes that caused deposition of Fe-rich olivine and Fe enrichment along cracks crosscutting pyroxene crystals. However, formation of these secondary phases seems to be independent of the degree of thermal metamorphism observed within every type of clast, which would support a late-stage metasomatism model for their formation.

INTRODUCTION

Howardite, eucrite, and diogenite (HED) meteorites represent the largest suite of achondrites currently known (Pun and Papike 1996), encompassing approximately 2213 classified meteorites according to the Meteoritical Bulletin (status November 18, 2019). This suite of rocks includes magmatic rocks and breccias, consisting of different lithologies and some minor exogenous impact materials (e.g., McSween et al. 2011). Similarities in oxygen isotopic compositions and crystallization ages as well as constant Fe/Mn-ratios of mafic minerals indicate a common place of origin for the vast majority of HEDs, most likely the asteroid 4-Vesta (Consolmagno and Drake 1977; Drake 1979, 2001; Binzel and Xu 1993; Papike 1998; De Sanctis et al. 2012). By analyzing their textures, mineralogies, and chemical compositions, indispensable information about formation and surface processes of 4-Vesta and differentiated asteroids in general can be gained. Furthermore, these petrographic studies can be directly compared to data derived from space missions such as NASA's DAWN mission and other remote sensing observations and therefore provide ground truth for such spectroscopic data (Binzel et al. 1997; Gaffey 1997; De Sanctis et al. 2012; McCoy et al. 2015).

In general, eucrites are composed of almost the same amount of rock-forming Mg-Fe-Ca pyroxene and Ca-rich plagioclase based on modal analyses of unbrecciated eucrites (Mayne et al. 2009), whereas the pyroxene composition varies significantly (Pun and Papike 1996). Eucrites can be further divided according to their

petrographic and compositional characteristics into basaltic rocks, gabbroic cumulates, and polymict eucrites (Miyamoto et al. 1978; Olsen et al. 1978; Takeda et al. 1978). Basaltic eucrites represent fine- to medium-grained rocks (<2 mm grain size; McSween et al. 2011) with ophitic to subophitic or vitrophyric textures that formed during fast cooling of a lava. Most basaltic eucrites experienced postmagmatic thermal metamorphism (Takeda and Graham 1991; Metzler et al. 1995; Yamaguchi et al. 1996), which resulted in equilibration of chemically zoned pyroxene crystals, silicate clouding, and subsolidus exsolution of augite lamellae within pigeonite hosts (Mittlefehldt et al. 1998). Cumulate eucrites are medium- to coarse-grained gabbroic rocks (Mittlefehldt et al. 1998; McSween et al. 2011), which have geochemical whole rock signatures that indicate they were initially igneous cumulates. Their pyroxenes are more enriched in Mg (En_{46-65}) compared with basaltic eucrites and are inverted pigeonite (orthopyroxene) in some cases due to thermal metamorphism.

The surfaces of differentiated asteroids such as 4-Vesta are heavily influenced by postcrystallization events such as magmatic activity, impact processes, space weathering, and probably secondary metasomatism. This combination of events resulted in a complex evolution of mineralogical and textural characteristics of crustal rocks and leads to the formation of complex breccias with fragments of different lithologies, present in the today's collection of HEDs (Metzler et al. 1995; Yamaguchi et al. 1996, 2001). Thus, polymict eucrites are breccias of eucrite rock fragments that may contain clasts of basaltic and/or cumulate eucrites as well as clasts of equilibrated and/or nonequilibrated fragments (Reid 1982; Score et al. 1982; Delaney et al. 1984a). The matrix of polymict eucrites varies from fine-grained, fragmented to glassy and finely crystallized (Bunch 1975). Polymict eucrites are of great importance for understanding crustal formation and modification processes on differentiated asteroids.

Some HED meteorites, with basaltic eucrites in particular, exhibit unusual veinlet-like textures as secondary Fe-enrichments and/or fayalitic olivines. They occur mostly along cracks crosscutting unequilibrated pyroxenes and may be accompanied by small amounts of anorthitic plagioclase as well as troilite, chromite, and apatite. These phases are clearly younger than the general magmatic history of the rock, but not due to terrestrial alteration. They likely form in response to metasomatic reactions, high temperature events, or a combination of both (Takeda et al. 1983a, 1994; Warren 2002; Roszjar et al. 2009, 2011; Barrat et al. 2011; Barrett et al. 2016; Pang et al. 2017; Patzer and McSween 2018). The topic of secondary alteration in eucrites and their possible relation to metasomatic activity on 4-Vesta are not the major focus of this study, but will be investigated in a second study on laboratory experiments in more detail.

This study investigates the petrographic and compositional characteristics of a suite of five polymict eucrite samples collected near the Antarctic Yamato Mountains that have not been characterized in much detail before. We have analyzed the textures, mineralogies, major element systematics, and secondary Fe-enrichments of these polymict eucrites to better constrain their evolution and to extend our knowledge of the complex crustal evolution on differentiated asteroids such as 4-Vesta.

SAMPLES AND ANALYTICAL TECHNIQUES

Five polished thick sections were used for analysis, four of them classified as polymict eucrites, from the Antarctic meteorite collection of the National Institute of Polar Research (NIPR) in Tokyo, Japan: Yamato (Y-) 74159,114; Y-75011,114; Y-82210,101; Y-74450,113 (Fig. 1). The fifth sample, Y-793548,66, is classified as a monomict eucrite according to the Meteoritical Bulletin, but we will show here that there is more than one lithology present. Thus, this sample likely represents another polymict eucrite. Eucrite textures were examined using a JEOL 6510-LA scanning electron microscope (SEM) equipped with a tungsten electron emitter, and a backscattered electron (BSE) detector at the Institut für Mineralogie in Münster, Germany. All investigations were performed at an accelerating voltage of 20 kV, a working distance of 10 mm, and a beam current of several nA.

Pyroxene and plagioclase major and minor element compositions were determined using a JEOL JXA-8530F electron probe microanalyzer (EPMA) at the Institut für Mineralogie in Münster, Germany, equipped with a field emission gun, a backscattered electron detector, and five wavelength-dispersive spectrometers. Selected points were analyzed on equilibrated and unequilibrated pyroxenes, plagioclases, secondary minerals, and glassy phases. Analyses were performed with an accelerating voltage of 15 kV, a beam current of 15 nA, varying beam diameters of 1–10 μm according to the sizes of examined phases, and using chemically well-defined natural and synthetic reference materials. Silicates were analyzed with peak counting times of 10 s and background counting times of 5 s. Regions of glassy phases were analyzed with a beam current of 5 nA, peak counting times of 5 s, background counting times of 3 s, and a slightly defocused beam to prevent volatilization of elements. All data were reduced by standard ZAF correction routines. Lithic clasts containing pyroxenes and plagioclases of different grain sizes were evaluated by analyzing five to six large pyroxene and plagioclase

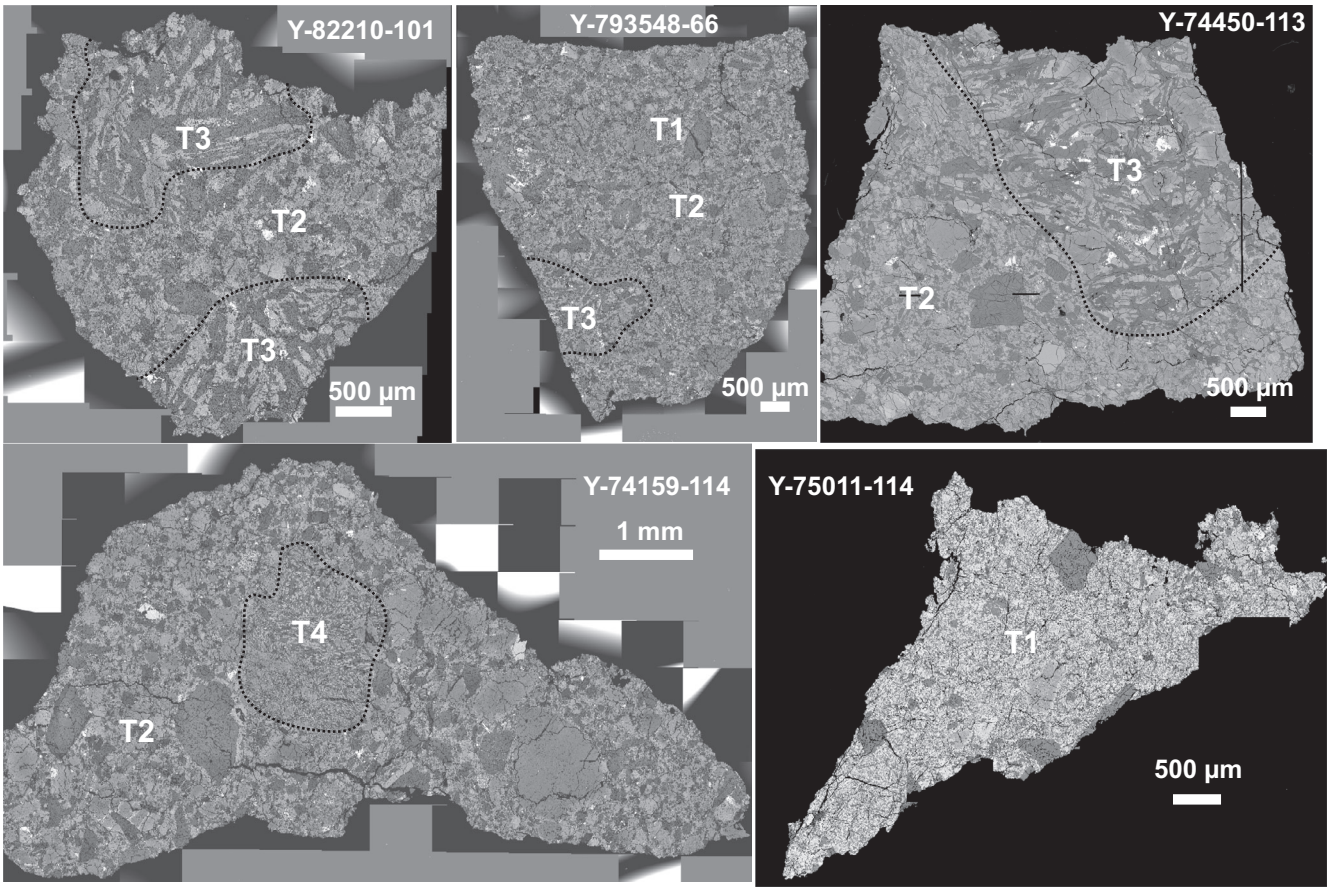

Fig. 1. BSE composite images of all five analyzed Yamato polymict eucrite breccias showing different clasts with distinct textures, marked by dashed lines, except for the texture "T2," which generally serves as the partially recrystallized matrix of the other textures. See text for details.

crystals at core and rim position with three to six points, respectively. This enabled a careful investigation of major element compositional zoning of some unequilibrated pyroxenes. Matrix areas were analyzed on average by single measurements of about 10 different crystals per phase. Secondary Fe-rich olivine was evaluated by analyzing one to five olivine crystals or veins with 3–21 analytical spots, respectively. To evaluate elemental concentration changes, the Fe-enrichments were analyzed by single point analyses and/or a series of points, forming a profile across the vein perpendicularly. Areas of heterogeneous glassy phases were analyzed with three to nine points to receive a mean value of the glasses. Detection limits for all major and minor elements are within the range 0.01–0.02 wt%.

RESULTS

Petrographic Investigations

All five Yamato meteorites represent strongly brecciated eucrites that exhibit different lithic clasts with a variety of basaltic mineralogies (pyroxene + plagioclase) and textures. All analyzed samples contain more than one predominant texture, with four dominant textures of individual clasts (Figs. 1–2): porphyritic ("T1"), brecciated and partially recrystallized ("T2"), subophitic ("T3"), and quench-textured ("T4"). The nature of these textures will be described in more detail below within the selected Yamato eucrites studied.

Y-75011,114 contains several coarse-grained, rounded pyroxene and plagioclase fragments (0.1–0.5 mm), set in a fine-grained (5–15 µm) ophitic groundmass composed of pyroxene and plagioclase material (T1, Fig. 1). Lath-shaped silica phases (up to 0.01 × 0.1 mm) are an essential part of matrix material and small grains of ilmenite and troilite appear sporadically. Glassy, devitrified, or partly recrystallized regions occur in some places. Large pyroxene grains are compositionally diverse with both zoned and equilibrated crystals. Some of the equilibrated crystals contain tiny inclusions (Fig. 3a) and sometimes exsolution lamellae of Cr-rich phases (<1 µm), most likely spinels.

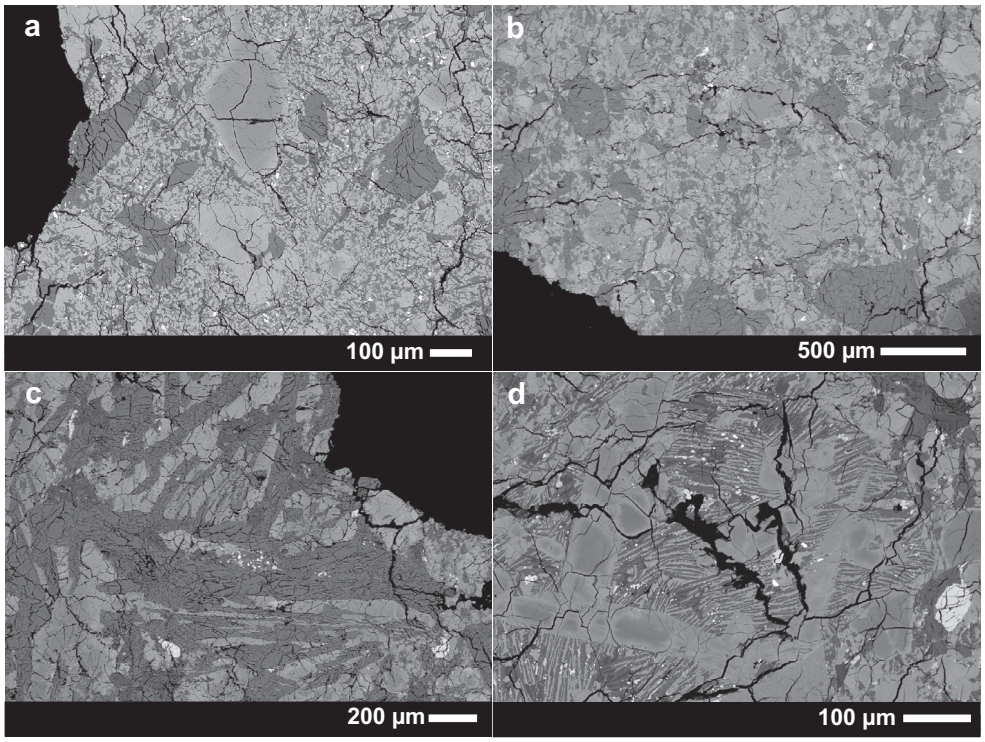

Fig. 2. BSE images of analyzed Yamato meteorites illustrating the four predominant textures: (a) T1: porphyritic (Y-75011 [shown here] and Y-793548), (b) T2: partially recrystallized fragmental breccia (Y-793548 [shown here], Y-793548, Y-82210, Y-74450), (c) T3: subophitic (Y-82210 [shown here], Y-793548, Y-74450), (d) T4: quench-textured (Y-74450 [shown here] and Y-74159).

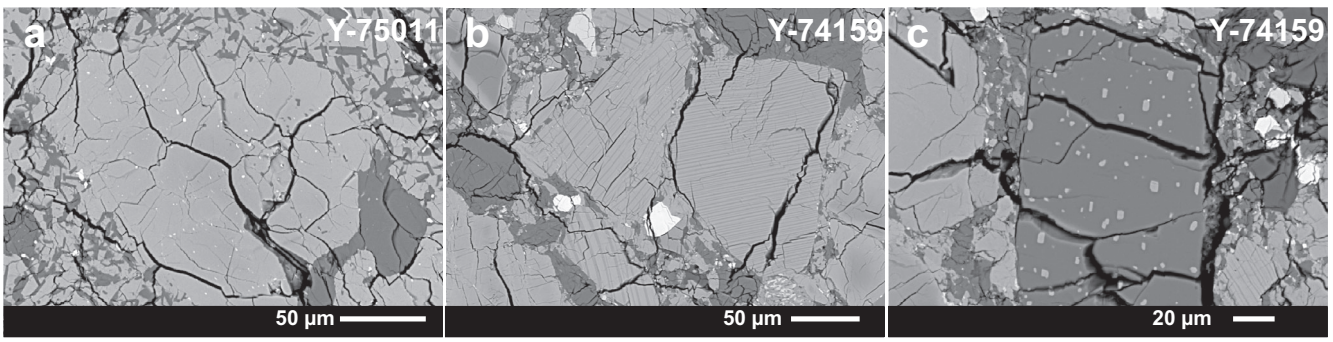

Fig. 3. BSE images of analyzed Yamato meteorites showing areas with signs of thermal alteration. a) Fe-Cr-Ti-rich exsolutions in an equilibrated pyroxene, (b) augite exsolution lamellae in pigeonite with different widths in close association, and (c) oriented pyroxene inclusions in plagioclase.

Except for Y-75011,114, all other analyzed meteorites contain large clasts with brecciated textures (T2, Fig. 2). These textures cover at least one half of the thick section and consist of large angular pyroxene and plagioclase fragments in varying sizes (up to 0.5 mm), set in fine-grained material composed predominantly of pyroxene and plagioclase minerals. Fragments of SiO_2 polymorph(s) and ilmenite (0.2 × 0.2 mm) occur as well as a part of this mineral assemblage. Furthermore, accessory phases such as olivine, troilite, chromite, areas of glass, dark mesostasis, and iron metal are present. Some pyroxenes show extensive chemical zoning, while others are equilibrated and show chemically homogeneous Mg/Fe ratios, some of which are slightly clouded and rarely contain exsolution lamellae of augite and sometimes very fine exsolutions along crystallographic planes of Cr-rich phases, most likely spinels. Some plagioclase

crystals exhibit pyroxene inclusions. Both chemically zoned as well as equilibrated pyroxenes exhibit ferroan olivine and Fe-enrichments as described for Y-75011.

Y-793548,66 consists predominantly of the brecciated texture (T2), but also contains small porphyritic (T1) and subophitic domains (T3, Fig. 2). Because of these different lithologies, this sample cannot be classified as a monomict eucrite anymore. Moreover, studied sections of Y-82210 and Y-74450 contain large clasts with medium-grained subophitic textures (T3). Plagioclase crystals are lath shaped (up to 0.2 × 1 mm) and their interstices are filled with chemically zoned and equilibrated pyroxenes. Silica (up to 0.2 mm) and ilmenite grains (up to 0.1 mm) as well as areas of dark mesostasis rich in silica, troilite, and iron metal are also present. In the case of Y-74450, some large pyroxene crystals are part of the subophitic texture and grains of ilmenite, chromite and silica as well as regions of mesostasis occur more frequently than in Y-82210. The pyroxene crystals of Y-82210 contain only few olivine veins, and Fe-enrichments are sporadically associated with chromite grains. In the case of Y-74450, Fe-enrichments and olivine phases occur more intensively and frequently within the larger pyroxene crystals (Fig. 4a).

Section Y-74159,114 is dominated by a large clast with brecciated texture as described above, but also contains a domain of the quench texture in the center of the investigated thin section (T4, Fig. 2). This region is characterized by compositionally zoned pyroxene phenocrysts (80 × 200 μm) embedded in a mass of small radiating lath-shaped pyroxene and plagioclase crystals (20 × 100 μm). Silica phases (up to 50 μm), small ilmenite, and iron metal grains (up to 10 μm) are a random, but essential part of this mineral assemblage. Slight Fe-enrichments along small cracks inside the pyroxenes are visible. Large plagioclase grains partly show small inclusions of pyroxene and Fe- and/or Ti-rich phases (Fig. 3c).

Veinlet-like Fe-enrichments and ferroan olivine in the investigated Yamato eucrites occur along pre-existing or healed cracks of some large zoned pyroxene crystals (Fig. 4). These structures are restricted to pyroxene crystals and end up abruptly at pyroxene grain boundaries (Fig. 4d). The olivine phases have an irregular but vein-like shape, resembling single or aligned pearls of single crystals with a width of ~10–20 μm. The grain boundaries of olivines are sharp and the adjacent pyroxene is mostly accompanied by a strong Fe-enrichment that decreases with increasing distance to the olivine vein (width ~6 μm). The olivine phases are sporadically accompanied by chromite, anorthitic plagioclase, and troilite grains (~10 μm). The secondary Fe-rich phases appear more frequently within pyroxenes within the brecciated texture and are not restricted to large crystals, but also occur along their grain boundaries between different pyroxene grains and between pyroxene and plagioclase grains (Fig. 4). Fe-enrichments do not only occur in contact with olivine phases but also alone as thin veins or thick regions within pyroxene crystals with varying Fe-content, which is all consistent with previous observations (e.g., Warren 2002; Barrat et al. 2011; Roszjar et al. 2011; Pang et al. 2017; Patzer and McSween 2018).

To conclude on the petrographic observations, all five eucrites contain four dominant lithic textures and mineral fragments with greatly varying abundances and metamorphic degrees, indicative of different thermal formation regimes and intense postmagmatic brecciation and metamorphism. In addition, secondary alteration is observed across almost all lithic textures and independent of the metamorphic degrees.

Chemical Composition of Pyroxene, Plagioclase, and Glassy Areas

Electron microprobe data of pyroxene, olivine, and plagioclase grains from all five Yamato meteorites are listed in Tables 1–3. Analyses of pyroxene and plagioclase grains indicate a similar chemical composition according to their specific textures, following the same compositional trends (see below). These chemical trends differ slightly among the four predominant textures, shown in Figs. 5–6. Pyroxene chemical zoning is observed petrographically by BSE imaging and confirmed by quantitative element analyses.

Results of all four dominant textures show distinctive igneous zoning from Mg-rich pigeonite cores to Fe-Ca-rich augite rims. Equilibrated grains are more enriched in Fe and Ca than the rims of chemically zoned grains. Chemical data from pyroxene rims and equilibrated pyroxene crystals vary more in composition, compared to core analyses. Thus, a wide range of compositions (Fe-rich, Ca-rich, Fe-Ca-rich, and Mg-rich) can be determined. Due to point analyses of core and rim positions of unequilibrated pyroxenes only, sampling of whole grains is discontinuous, resulting in some interceptions in the given Fe-Mg-Ca-trends of the pyroxene quadrilateral diagrams (Fig. 5). Pyroxene rims are typically low in Ca. However, rim data of lithologies T3 and T4 scatter more strongly, and are more Ca-rich compared to pyroxenes derived from textures T1 and T2 (Fig. 5). Equilibrated pyroxenes are mostly enriched in Ca. Equilibrated pyroxenes of the brecciated texture scatter over a wide compositional field compared to data of all other textures.

Plagioclase compositions vary from An_{71} to An_{95} and follow a slightly K-depleting trend with no chemical zoning (Fig. 6). Furthermore, data from core,

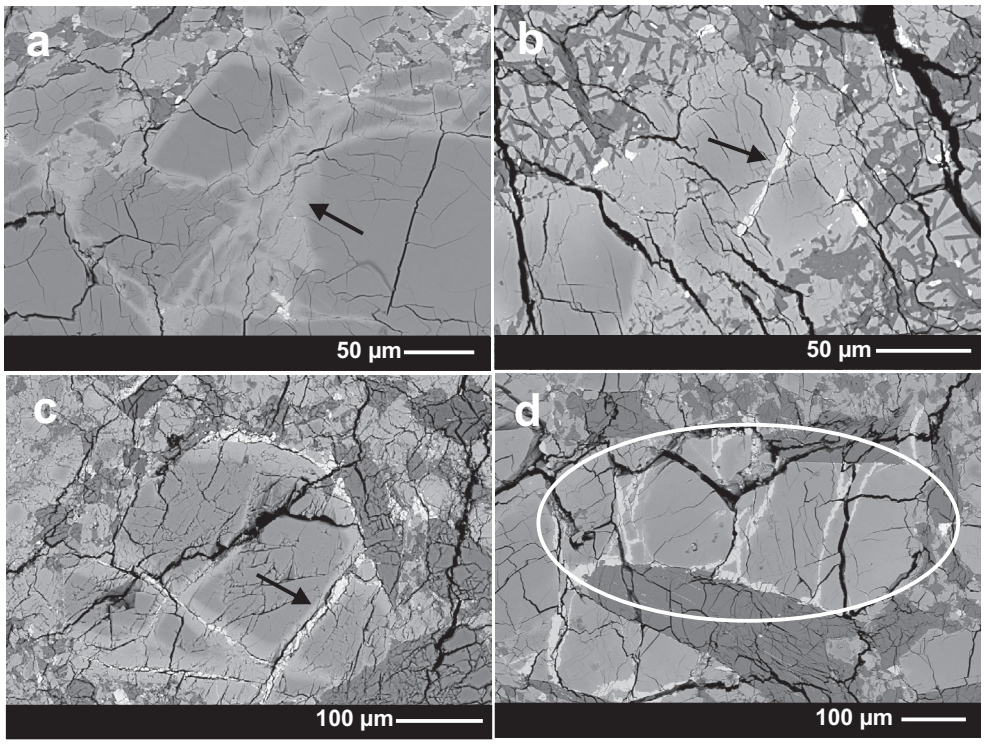

Fig. 4. BSE images of the analyzed Yamato meteorites showing prominent Fe enrichments to varying intensities. a) Y-74450. Fe enrichments along cracks within pyroxenes (arrow). b) Y-75011. Well-developed fayalite vein (arrow) crosscutting a pyroxene. c) Y-82210. Fe enrichments as well as clearly developed fayalite veins (arrow) within a single pyroxene. d) Y-74159. Fayalite veins crosscutting pyroxenes and ending at the boundaries of the plagioclase crystals (encircled).

rim, and small matrix grains have a consistent chemical range. Data in the porphyritic and brecciated textures show a greater variability compared to larger crystals of quench and subophitic textures.

In all five Yamato polymict eucrites, we observe heterogeneous regions of partly recrystallized melt pools (T4, Fig. 7), sometimes as large areas or as fragments within the brecciated texture T2. Their textures are complex and fine-grained, from glassy "Schlieren" and cryptocrystalline to fine crystalline. Some of these clasts contain altered mineral fragments, for example, surrounding silicates, phosphates, and/or sulfides. Other regions show skeletal devitrification textures with varying patterns. Due to their fine-grained heterogeneous appearance, quantification of chemical compositions of these regions bears large uncertainties. However, considering major elements only, our analyses indicate a mean composition relative to the corresponding surrounding silicates in all samples (Fig. 8).

DISCUSSION

Petrography

Characterization of all investigated polymict eucrites revealed a complex petrography, containing a variety of lithologies indicating diverse physical–chemical evolution of the host rocks. The porphyritic texture of the lithic clast T1 most likely represents a rapidly cooled melt, which crystallized to a fine-grained, mainly ophitic material. The high temperatures and fast cooling times needed to form such a texture were most likely generated by impacts, because a primary melt would not generate such a variety of different porphyritic clasts. Due to high impact energy, mineral clasts of different surrounding places were ejected into a liquid melt before solidifying. This would explain observed compositional and structural variations of the pyroxene crystals within this type of texture. Although other studies of Y-75011 (e.g., Takeda et al. 1994; Pun and Papike 1996; Barrat et al. 2011) did not report on the occurrence of this texture, Metzler et al. (1995) described similar findings for the howardite Elephant Moraine (EET) 87503.

Lithologies of brecciated texture (T2) represent breccias of mineral fragments with different origins or thermal evolution. The mineral grains of this lithology exhibit a variety of features that indicate thermal annealing to varying degree as well as mechanical stress (Pun and Papike 1996). The brecciated texture (T2) was described in several eucrites of other studies, for example, in Y-82210 (e.g., Graham and Yanai 1986;

Table 1. Average microprobe analyses in wt% of representative pyroxene grains from analyzed textures T1–4.

Comment/ Sample	MgO	SiO_2	Al_2O_3	CaO	FeO	TiO_2	Cr_2O_3	MnO	Total	Endmembers (avg)	Endmembers (range)
T1 (Y-75011)											
Core (n = 29)	22.1	52.1	1.33	2.89	19.3	0.19	0.77	0.69	99.36	$En_{63.1}Fs_{30.9}Wo_{5.9}$	$En_{57.0\text{-}68.4}Fs_{27.2\text{-}35.6}Wo_{4.1\text{-}8.4}$
σ	1.60	0.87	0.29	0.56	1.30	0.06	0.16	0.06			
Rim (n = 38)	13.7	49.2	1.08	3.60	29.3	0.33	0.46	0.91	98.60	$En_{41.9}Fs_{50.3}Wo_{7.8}$	$En_{32.0\text{-}54.0}Fs_{41.4\text{-}60.2}Wo_{3.3\text{-}16.3}$
σ	2.00	1.00	0.29	1.30	2.00	0.15	0.15	0.11			
Eq (n = 27)	9.40	48.4	1.17	10.1	28.1	0.64	0.39	0.90	99.11	$En_{29}Fs_{48.7}Wo_{22.3}$	$En_{24.0\text{-}44.2}Fs_{41.3\text{-}54.6}Wo_{6.5\text{-}31.4}$
σ	1.40	0.43	0.17	2.40	2.20	0.16	0.08	0.07			
Matrix (n = 9)	9.67	48.2	0.73	6.43	31.9	0.55	0.22	1.06	98.80	$En_{30.1}Fs_{55.6}Wo_{14.4}$	$En_{28.7\text{-}32.1}Fs_{54.3\text{-}57.4}Wo_{13.0\text{-}15.6}$
σ	0.35	0.38	0.12	0.38	0.55	0.12	0.05	0.03			
T2 (Y-82210)											
Core (n = 20)	22.6	52.9	1.20	2.67	19.2	0.16	0.79	0.66	100.20	$En_{64.1}Fs_{30.5}Wo_{5.4}$	$En_{55.1\text{-}72.0}Fs_{24.9\text{-}8.9}Wo_{3.2\text{-}8.9}$
σ	2.20	0.71	0.19	0.75	1.80	0.04	0.15	0.10			
Rim&eq (Fe-rich) (n = 34)	13.7	49.6	0.91	2.54	31.3	0.22	0.46	0.97	99.76	$En_{41.5}Fs_{53.0}Wo_{5.5}$	$En_{35.9\text{-}52.9}Fs_{43.3\text{-}57.9}Wo_{2.0\text{-}11.6}$
σ	1.50	0.64	0.40	0.96	1.90	0.06	0.23	0.10			
Rim&eq (Ca-rich) (n = 12)	12.0	49.3	1.22	7.60	27.5	0.48	0.54	0.90	99.56	$En_{36.5}Fs_{46.9}Wo_{16.6}$	$En_{33.1\text{-}42.6}Fs_{43.2\text{-}51.4}Wo_{8.8\text{-}23.1}$
σ	1.10	0.82	0.47	2.30	1.40	0.11	0.09	0.04			
Rim&eq (Fe-Ca-rich) (n = 4)	5.50	47.6	1.03	10.60	32.8	0.87	0.24	1.00	99.71	$En_{17.5}Fs_{58.3}Wo_{24.2}$	$En_{8.6\text{-}24.2}Fs_{50.5\text{-}68.3}Wo_{22.1\text{-}26.2}$
σ	2.20	0.54	0.15	0.91	3.50	0.16	0.19	0.11			
T3 (Y-793548)											
Core (n = 20)	22.7	52.6	1.45	2.77	19.1	0.17	0.75	0.66	100.17	$En_{64.1}Fs_{30.3}Wo_{5.6}$	$En_{58.4\text{-}68.0}Fs_{27.8\text{-}33.6}Wo_{4.2\text{-}9.0}$
σ	1.20	0.63	0.50	0.58	0.85	0.06	0.14	0.04			
Rim (n = 14)	13.4	49.5	1.19	4.40	29.3	0.32	0.50	0.93	99.58	$En_{40.7}Fs_{49.8}Wo_{9.5}$	$En_{33.9\text{-}48.8}Fs_{44.2\text{-}59.9}Wo_{2.7\text{-}17.8}$
σ	1.80	0.61	0.43	2.10	2.70	0.13	0.16	0.10			
Eq (n = 5)	10.1	49.2	1.30	8.40	28.9	0.54	0.50	0.93	100.02	$En_{31.3}Fs_{50.1}Wo_{18.6}$	$En_{26.4\text{-}37.9}Fs_{46.5\text{-}56.8}Wo_{9.0\text{-}23.4}$
σ	1.10	0.44	0.25	2.00	1.60	0.25	0.14	0.05			
σ	0.52	0.35	0.37	1.40	1.70	0.15	0.07	0.08			
T4 (Y-74450)											
Core (n = 13)	23.7	52.0	1.37	2.35	17.9	0.16	0.84	0.61	98.94	$En_{66.8}Fs_{28.4}Wo_{4.8}$	$En_{60.2\text{-}71.2}Fs_{25.2\text{-}32.4}Wo_{3.6\text{-}7.4}$
σ	1.50	0.55	0.22	0.56	1.30	0.06	0.17	0.06			
Rim (n = 13)	13.0	48.4	2.00	5.70	27.4	0.42	0.76	0.86	98.60	$En_{39.9}Fs_{47.4}Wo_{12.7}$	$En_{33.6\text{-}48.5}Fs_{29.0\text{-}57.4}Wo_{2.2\text{-}31.1}$
σ	1.30	0.66	1.60	5.10	6.30	0.27	0.45	0.17			
Needle (n = 4)	9.37	47.5	1.14	7.30	30.7	1.02	0.15	1.01	98.23	$En_{29.4}Fs_{54.1}Wo_{16.5}$	$En_{28.3\text{-}32.0}Fs_{51.8\text{-}58.1}Wo_{13.3\text{-}19.5}$
σ	0.57	0.36	0.18	1.40	1.50	0.32	0.01	0.09			

n, number of measured points; eq., equilibrated.

Table 2. Average microprobe analyses in wt% of representative olivine grains and Fe-enriched pyroxene veins from analyzed textures T1–4.

Comment/Sample	MgO	SiO_2	Al_2O_3	CaO	FeO	TiO_2	Cr_2O_3	MnO	Total	Endmembers (avg)	Endmembers (range)
T1 (Y-75011)											
Olivine (n = 4)	10.1	31.4	n.d.	0.04	55.9	0.01	0.06	1.30	98.90	$Fo_{24.5}Fa_{75.5}$	$Fo_{24.1\text{-}24.7}Fa_{75.3\text{-}75.9}$
σ	0.16	0.24		0.03	0.10	0.02	0.04	0.06			
T1 (Y-793548)											
Fe-enr (n = 8)	13.8	49.7	0.90	2.63	30.8	0.37	0.78	0.96	100.04	$En_{41.8}Fs_{52.5}Wo_{5.7}$	$En_{38.8\text{-}45.0}Fs_{50.0\text{-}55.1}Wo_{4.3\text{-}8.0}$
σ	0.65	0.68	0.17	0.64	1.20	0.14	0.72	0.07			
T2 (Y-82210)											
Olivine (n = 14)	8.47	31.5	0.27	0.15	57.4	0.04	0.11	1.33	99.39	$Fo_{20.8}Fa_{79.2}$	$Fo_{19.2\text{-}23.8}Fa_{76.2\text{-}80.8}$
σ	0.52	1.00	0.76	0.26	0.99	0.04	0.11	0.09			
Fe-enr (n = 31)	13.1	50.7	0.94	1.76	32.3	0.10	0.48	1.01	100.39	$En_{40.4}Fs_{55.7}Wo_{3.9}$	$En_{38.6\text{-}43.1}Fs_{52.9\text{-}58.4}Wo_{3.1\text{-}4.6}$
σ	0.87	1.20	0.16	0.35	1.50	0.02	0.05	0.12			
T3 (Y-793548)											
Olivine (n = 6)	10.3	32.2	n.d.	0.07	56.1	0.13	0.07	1.26	100.24	$Fo_{24.7}Fa_{75.3}$	$Fo_{23.3\text{-}29.8}Fa_{70.2\text{-}76.7}$
σ	1.10	0.58		0.05	1.70	0.06	0.03	0.09			
Fe-enr (n = 7)	13.8	49.2	1.28	2.90	30.5	0.18	0.56	0.97	99.53	$En_{41.8}Fs_{51.8}Wo_{6.4}$	$En_{38.8\text{-}60.1}Fs_{34.3\text{-}55.5}Wo_{3.8\text{-}13.3}$
σ	0.99	1.10	0.34	1.50	2.20	0.08	0.11	0.06			
T4 (Y-74159)											
Fe-enr (n = 6)	13.4	48.0	2.47	4.06	28.5	0.29	0.94	0.84	98.54	$En_{41.4}Fs_{49.6}Wo_{9.0}$	$En_{38.4\text{-}45.7}Fs_{44.7\text{-}52.4}Wo_{6.7\text{-}12.2}$
σ	1.00	0.62	0.53	0.86	1.50	0.12	0.28	0.07			

n, number of measured points; Fe-enr, Fe-enriched; n.d., below detection limit.

Yamaguchi and Takeda 1992), Y-74159, and Y-74450 (Takeda and Yanai 1982; Delaney et al. 1984b). Metzler et al. (1995) described a clastic matrix containing angular, clearly fragmented, and comminuted mineral grains to be the result of mechanical stress.

The formation of the subophitic texture (T3) was discussed by Pun and Papike (1996) to be the result of a fast cooling melt. This textural type was also found, for example, in the eucrites Millbillillie, Camel Donga, Allan Hills (ALHA) 78132 (Metzler et al. 1995), Y-75011, Pasamonte, Northwest Africa (NWA) 5073 (Roszjar et al. 2011), and NWA 049 (Barrat et al. 2011).

The quench-textured lithology (T4) is very rare among eucritic meteorites. It could be the result of fast cooling, cotectically crystallizing silicates after intrusion of a shock-induced melt into the solid host rock followed by rapid cooling (Bobe 1992; Metzler et al. 1995; Warren et al. 1996). However, the heavily cratered surface of 4-Vesta induced by impact gardening of its crust contradicts the limited number of samples that show these features. We therefore consider a certain geological setting, for example, below the center of a crater, where a specific and spatially restricted temperature and pressure regime occurs, can lead to the formation of this unusual lithology. Furthermore, it is also possible that this lithology represents a fragment of a quenched surface on a lava flow.

Lithologies with the same petrographic characteristics among the basaltic eucrites are assumed to have a common origin and/or thermal-metamorphic evolution. Furthermore, the parental melt chemical compositions can be derived from core compositions of major minerals and should be similar in such a case, as observed here (Figs. 5 and 6). Thus, eucrites that contain fragments with the same or very similar petrographic and mineralogical characteristics are considered as paired rocks (Pun and Papike 1996; Buchanan and Mittlefehldt 2003; Beck et al. 2012; Lunning et al. 2016; this study). The petrographic investigations of all five Yamato meteorites in this study revealed four dominating textures (porphyritic, brecciated, subophitic, and quench-textured) that occur within several samples. Therefore, this observation provides strong evidence that these meteorites genetically belong together and formed under similar conditions involving at least partially similar source melt compositions.

Furthermore, literature data indicate that other sections of the same eucrites, with polymict samples in particular, show significantly different textures (e.g., Pun and Papike 1996), implying highly heterogeneous

Table 3. Average microprobe analyses in wt% of representative plagioclase grains from analyzed textures T1–4.

Comment/Sample	Na_2O	MgO	SiO_2	Al_2O_3	K_2O	CaO	FeO	BaO	Total	Endmembers (avg)	Endmembers (range)
T1 (Y-75011)											
Large (n = 38)	1.51	0.08	48.1	32.3	0.16	16.6	0.60	0.09	99.50	$An_{85.0}Ab_{14.0}Or_{1.0}$	$An_{71.5\text{-}94.4}Ab_{5.3\text{-}25.9}$ $Or_{0.1\text{-}3.3}$
σ	0.71	0.04	2.40	1.70	0.14	1.50	0.35	0.06			
Small (n = 4)	1.86	0.08	49.2	31.6	0.16	15.9	0.93	0.10	99.94	$An_{81.7}Ab_{17.3}Or_{1.0}$	$An_{79.6\text{-}83.3}Ab_{15.9\text{-}19.2}$ $Or_{0.8\text{-}1.2}$
σ	0.17	0.02	0.66	0.47	0.03	0.28	0.12	0.02			
Matrix (n = 7)	1.90	0.04	49.2	31.9	0.18	15.8	0.92	n.d.	100.06	$An_{81.3}Ab_{17.6}Or_{1.1}$	$An_{78.2\text{-}83.5}Ab_{15.8\text{-}20.4}$ $Or_{0.8\text{-}1.6}$
σ	0.19	0.02	0.70	0.55	0.05	0.26	0.06				
T2 (Y-793548)											
Large (n = 48)	1.33	0.07	48.2	32.6	0.12	17.2	0.58	0.08	100.28	$An_{87.0}Ab_{12.2}Or_{0.8}$	$An_{76.2\text{-}91.9}Ab_{7.7\text{-}22.2}$ $Or_{0.2\text{-}2.0}$
σ	0.46	0.03	1.70	1.40	0.08	1.00	0.36	0.05			
Small (n = 10)	2.01	n.d.	50.6	30.5	0.27	15.7	1.12	0.06	100.58	$An_{79.9}Ab_{18.5}Or_{1.6}$	$An_{75.6\text{-}85.3}Ab_{14.0\text{-}21.7}$ $Or_{0.7\text{-}2.7}$
σ	0.26		1.00	1.00	0.11	0.70	0.51	0.04			
Matrix (n = 8)	1.55	0.08	49.1	32.2	0.15	16.9	0.98	n.d.	101.08	$An_{85.0}Ab_{14.1}Or_{0.9}$	$An_{80.5\text{-}92.3}Ab_{7.4\text{-}18.1}$ $Or_{0.3\text{-}1.4}$
σ	0.41	0.03	1.70	1.20	0.06	0.93	0.26				
T3 (Y-82210)											
Plagioclase (n = 56)	1.87	n.d.	49.2	31.3	0.50	15.7	0.93	n.d.	100.32	$An_{79.9}Ab_{17.2}Or_{2.9}$	$An_{77.3\text{-}89.6}Ab_{9.2\text{-}20.7}$ $Or_{0.6\text{-}2.4}$
σ	0.31		6.60	2.70	2.00	2.20	0.36				
T4 (Y-74159)											
Plagioclase (n = 10)	1.96	0.09	50.0	30.9	0.22	15.5	1.05	0.11	99.95	$An_{80.3}Ab_{18.3}Or_{1.4}$	$An_{72.8\text{-}95.4}Ab_{4.4\text{-}24.3}$ $Or_{0.2\text{-}2.9}$
σ	0.60	0.07	1.40	1.10	0.13	0.96	0.24	0.08			

n, number of measured points; n.d., below detection limit.

mixing of genetically unrelated lithic fragments on a centimeter scale. A similar argument has been used to explain petrographic heterogeneity among different sections from the Pecora Escarpment Icefield (PCA) 02 howardite group, which also exhibit varying textures and lithologies among the paired samples (Beck et al. 2012). There it has been shown that the PCA 02 howardite group contains silicate mineral compositions spanning across the known compositional range of HEDs, which suggests that they derived from diverse source regions on Vesta, and that the Vestan regolith layer is not well mixed, that is, homogenized upon impact gardening. Therefore, comparing our results to data derived from thick sections of other studies of the same samples is not possible due to the complexity of the polymict eucrite petrography. Thus, we suggest that thick sections even of the same eucrite sample should be examined very carefully before comparison to other meteorites (Table 4).

To conclude, the suite of polymict eucrites studied here contains lithified fragments and clasts with complex lithic textures that formed under varying conditions within the host parent body, that are mixed together in respective meteorite samples. In view of recent spectral data of the DAWN mission, it was shown that Vesta is thoroughly blanketed by fragmental and locally heterogeneous regolith, which can be directly related to HED breccia mineralogies (De Sanctis et al. 2012). In addition, ejected and re-accumulated crustal material on Vesta by a proposed hit-and-run collision (Haba et al. 2019) might also account for the chemical and textural diversity preserved in polymict eucrites and howardites in particular. Therefore, all polymict eucrites studied record a complex sequence of brecciation, impact metamorphism, thermal annealing, and secondary alteration.

Pyroxene and Plagioclase Composition and Classification of Lithologies

Pyroxenes are dominant phases in eucrites and sensitive recorders of variables such as changes in chemical composition (e.g., equilibration) and shock

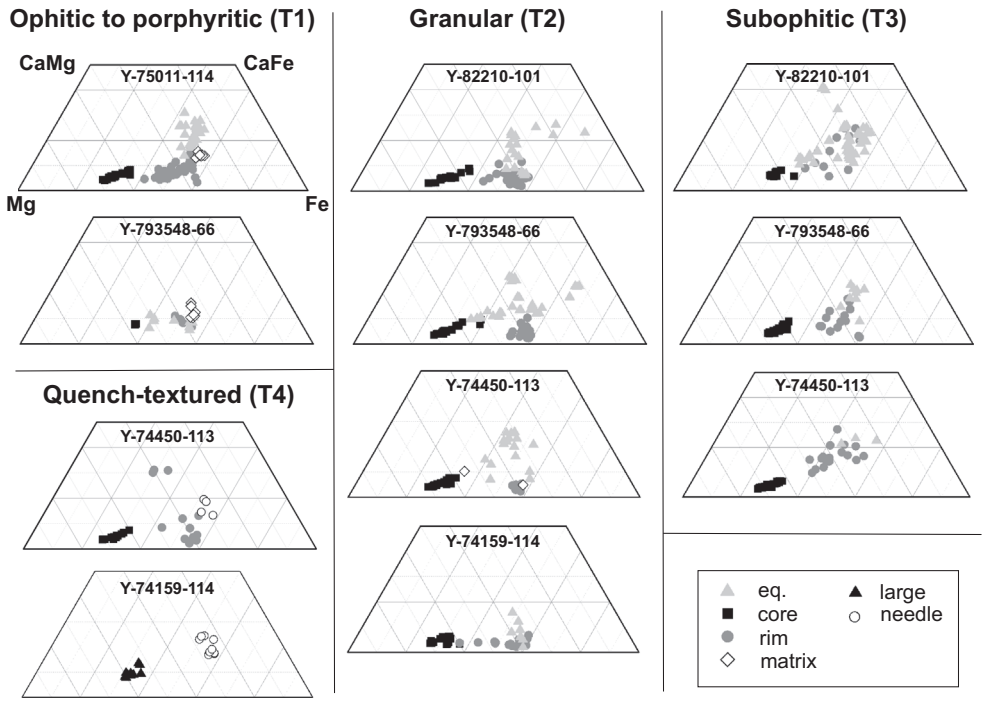

Fig. 5. Pyroxene quadrilateral diagrams (endmember compositions defined in the first panel) for mineral fragments within distinct lithologies, occurring within all five analyzed Yamato meteorites, ordered by the predominant four textures (T1–4).

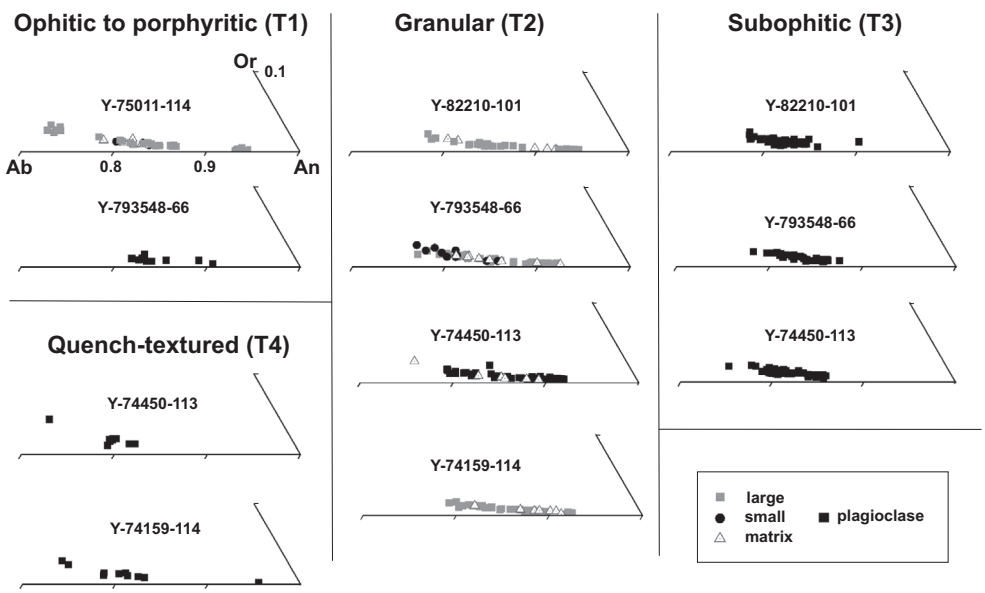

Fig. 6. Portions of the plagioclase ternary diagrams (endmember compositions defined in the first panel) for mineral fragments within distinct lithologies, occurring within all five analyzed Yamato meteorites, ordered by the predominant four textures (T1–4). Plagioclases with no further distinction according to grain size were simply named "plagioclase" (such as in textures T3 and T4).

metamorphism. Results from our quantitative elemental analyses of pyroxenes show a striking trend from Mg-rich pigeonite in the core to Fe-Ca-rich augites in the rim and in equilibrated crystals (Fig. 5). Takeda et al. (1983a) identified three trends of primary chemical zoning in pyroxene crystals, found in relatively fast cooled basaltic eucrites. According to these trends, our data of quench-textured (T4) and subophitic (T3)

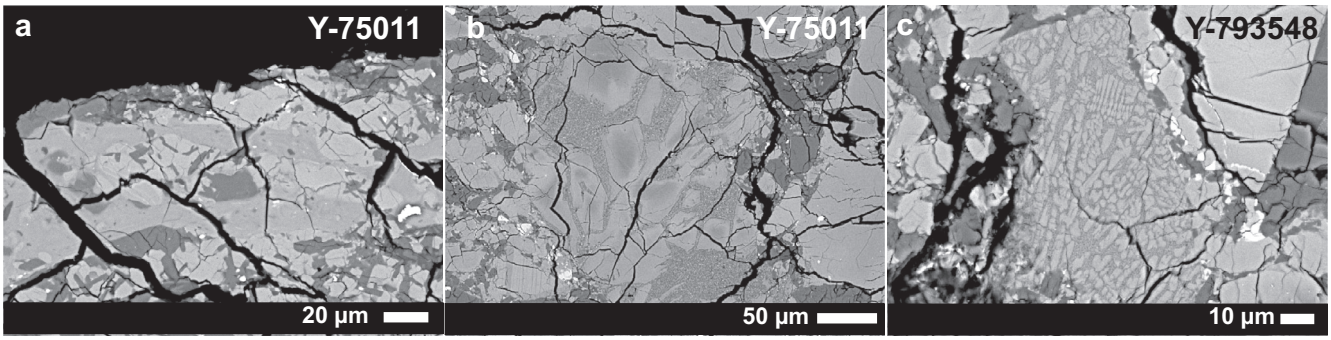

Fig. 7. Glassy areas and quench textures observed in Yamato meteorites: (a) "schlieren," (b) cryptocrystalline, fine crystalline, (c) devitrification textures.

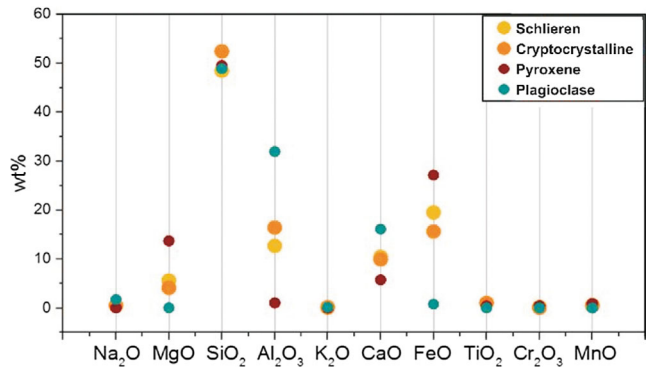

Fig. 8. Chemical composition of a representative recrystallized glassy area from Y-75011 (yellow) and cryptocrystalline areas (orange) in wt%, compared to average pyroxene (red) and plagioclase (blue) values within the same clast where the impact melt is embedded. Note that glass compositions are intermediate to rock forming silicates. (Color figure can be viewed at wileyonlinelibrary.com.)

textures follow a continuous Mg-Fe-Ca-trend. Zoned pyroxenes of the brecciated texture (T2) reflect an igneous Mg-Fe-trend, while equilibrated, homogeneous grains are more enriched in Ca, probably due to the presence of augite lamellae. The porphyritic texture (T1) of eucrite Y-75011 follows the Mg-Fe-Ca-trend as well.

Both the bulk chemistry of basaltic source melt and the pyroxene crystal growth conditions (e.g., degree of supercooling, cooling rate, and nucleation rates) are the most relevant parameters known to cause chemical zoning. Thus, either a slow and continuous cooling rate, or a long-lasting equilibration process (e.g., caused by a secondary high-temperature event) may be responsible for the lack of chemical zoning (Takeda and Yanai 1982; Takeda et al. 1983b). Chemical data of all pyroxene cores plot in the same region of composition, regardless of their texture (Fig. 5). This is strong evidence for both similar initial magmatic formation conditions on the eucrite parent body, and common bulk chemical compositions of the source melt. Great variation in composition instead would express a different origin of single mineral grains.

The plagioclase primary chemical composition encompasses values of An_{71-95} and therefore plots in the compositional field of known basaltic eucrite material with An_{71-98} (e.g., Mittlefehldt et al. 1998; Mayne et al. 2009; Barrat et al. 2011; Mittlefehldt 2015). Considering the plagioclase ternary diagrams, our sample set shows low concentration and little variation in K, indicative for a K depletion of the source melt (Fig. 6). Furthermore, compositions of distinct textures show a different extent in variation. Fragments with brecciated (T2) or porphyritic (T1) textures indicate a larger extent in compositional variation, likely due to occurrence of single plagioclase crystals as external fragments within the porphyritic texture deriving from more diverse origins than the ophitic groundmass in which they are embedded. On the contrary, both the quench-textured (T4) and subophitic (T3) textures show little variations in crystal composition. This may be due to a variety of factors such as source melt compositions and cooling rate. However, the still rather limited variation in crystal chemistry of rock-forming minerals in the investigated samples is indicative of chemically relatively similar host rock sources (Fig. 6).

Based on the concept proposed by Papike et al. (2003), the molar Fe/Mn-ratios of mafic minerals can be used to test the assumption whether investigated eucritic clasts have a common origin. Following this approach, we only used pyroxene crystal data due to the minor amount of olivine present in the current sample set of HEDs. As expected, all eucrite data are located around the compositional field of 4-Vesta defined by Papike et al. (2003), where a large suite of planetary plagioclase and pyroxene data of HED meteorites have been compiled. In general, elemental concentrations within major rock-forming minerals of all analyzed eucrites show abundances known for Vestan basaltic rocks. However, some analytical results of pyroxene and

Table 4. Occurrences of the four dominating textures in several HED meteorites. Listed are Yamato meteorites from this study and other work.

Texture	Petrography	This study	Other studies	References
T1	Porphyritic	Y-75011	EET 87503	Metzler et al. (1995)
		Y-793548		
		Y-74450		
T2	Brecciated	Y-793548	Y-82210	Graham and Yanai (1986)
		Y-82210		Yamaguchi and Takeda (1992)
		Y-74159	Y-74159	Delaney et al. (1984a)
		Y-74450	Y-74450	Takeda and Yanai (1982)
T3	Subophitic	Y-793548	Y-82210	Pun and Papike (1996)
		Y-82210	Y-74450	
		Y-74450	Millbillillie	Metzler et al. (1995)
			Camel Donga	
			ALHA 78132.92	
			Y-75011	Barrat et al. (2011)
			Pasamonte	
			NWA 049	
T4	Quench-textured	Y-74159	Stannern	Metzler et al. (1995)
		Y-74450		

plagioclase composition overlap with known cumulate material, also observed by Patzer and McSween (2012, 2018). In our case, only core data of zoned pyroxene grains and a few plagioclase grains of clasts showing brecciated and porphyritic textures match the cumulate composition. To discriminate between cumulate and basaltic material, Mayne et al. (2009) used the molar Fe/Mn- over Fe/Mg-ratios of pyroxenes. Their results reveal that cumulate material shows less scatter and is more restricted with respect to the Fe/Mg-ratio with values of 0.5 ± 0.2 when compared to basaltic material that spread over a wider compositional range. In the case of the five Yamato meteorites investigated here, we used all data of pyroxenes that show a clear igneous zoning (core and rim) to minimize any contribution from thermally metamorphosed or equilibrated material. Data of each eucrite clast overlap and vary largely in their Fe/Mg-ratios (Fig. 9). Thus, according to Mayne et al. (2009), the eucrite material exhibits a typical behavior of basaltic material. However, some pyroxene core data are rich in MgO and overlap with cumulate eucrite molar Fe/Mg-ratios of 0.5 ± 0.2. Due to the lack of bulk rock composition of the samples studied here, further chemical classification of the investigated basaltic polymict eucrites and assignment to the Main Group-Nuevo Laredo, Stannern-trend, or residual eucrite subdivisions according to proposed classification schemes (Stolper 1977; Barrat et al. 2007; Yamaguchi et al. 2009) is not possible here. However, it has been shown that the majority of polymict breccias have compositions consistent with mixtures of Main-Group eucrites and diogenites, with only some Stannern-trend basalts (Mittlefehldt 2015). This is also true for bulk rock compositions of the studied Yamato eucrites, where mg# and Ti contents show that these samples plot within the Main-Group field, with only some extending into the Stannern-trend field (Mittlefehldt 2015).

Thermal and Impact Metamorphism and Secondary Alteration

Due to the widespread occurrence of thermally metamorphosed samples among the HED suite of rocks, some authors argue for a global metamorphism process of crustal rocks on 4-Vesta (e.g., Takeda and Graham 1991; Yamaguchi et al. 1996; Schwartz and McCallum 2005). An effective heating source to cause igneous activity may have been induced by decay of the short-lived isotope ^{26}Al and impact events, with the latter mostly causing local heating and melting (Keil et al. 1997; Yamaguchi et al. 1997). Episodic formation of basaltic magma may also result from continuous heat production lasting over several million years, given an isolating lid such as early formed lava flows to retain the heat (Takeda 1997; Roszjar et al. 2016).

Metzler et al. (1995) assumed that observed diverse lithologies in HEDs are generated through the interaction of impact processes with crystallizing magma including rock pulverization, transport, mixing of different materials, melt formation, thermal shock, and mixing of surfaces with exogenic material. The Yamato meteorites analyzed here show a variety of textures that indicate both shock events and postmagmatic annealing likely induced by heating due to ^{26}Al decay. These post-magmatic features occur in different intensities, varying

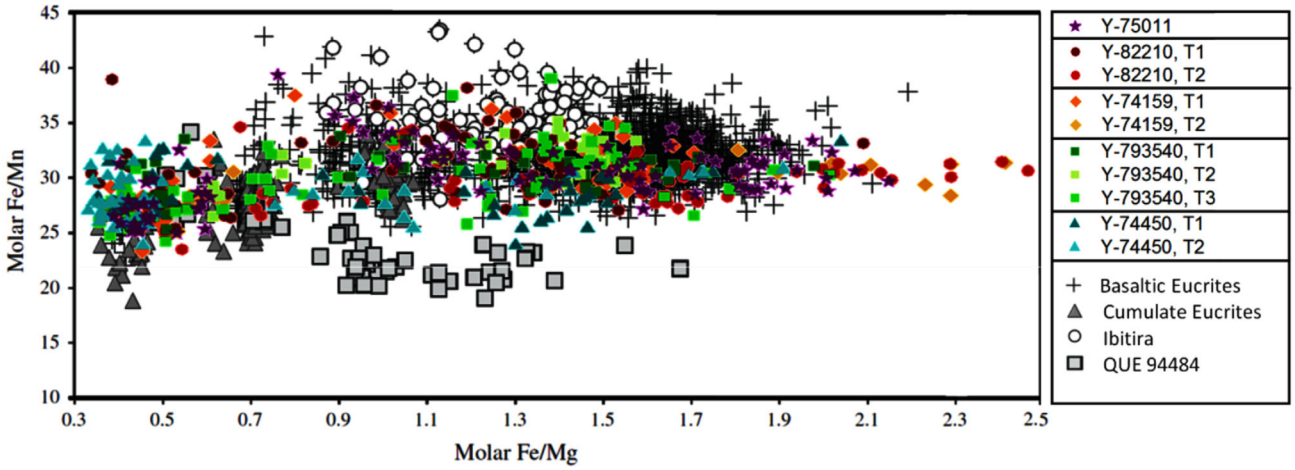

Fig. 9. Pyroxene molar Fe/Mn and Fe/Mg ratios of nonbrecciated eucrites of Mayne et al. (2009; black and gray data) compared to those from Yamato meteorites from this study (colored). (Color figure can be viewed at wileyonlinelibrary.com.)

from clast to clast, and even among coexisting mineral fragments. Metzler et al. (1995) developed a model of six phases considering the thermal and impact metamorphic evolution of HED meteorites that we can still well apply to the Yamato samples studied here, although more recent work recognized that thermal overprinting by heat from radioactive decay might affect the thermal evolution of eucrites in particular (e.g., Yamaguchi et al. 1996). Evolution of HEDs is therefore highly complex and in most cases difficult to interpret due to such multiple thermal metamorphism or/and impact brecciation events. For instance, impact glasses in Y-75011,114 contain zoned (crystallization of primary magmas—Phase I) but also equilibrated (low subsolidus cooling or reheating—Phase II) pyroxenes that were mixed together into a melt during brecciation (Phase III). A second impact event (Phase V) caused brecciation of the clast and formed, for example, "schlieren"-like areas. Similarly, clasts with brecciated textures contain zoned (Phase I) and equilibrated (Phase II) pyroxenes that were brought together during impact brecciation (Phase III). During a period of thermal metamorphism (Phase IV), material was compacted and small amounts of melts were formed. Rocks of subophitic textures experienced only slight metamorphism (Phase II) before brecciation. Quench-textured lithologies were brecciated without any metamorphic overprint.

Large mineral fragments in impact melt of Y-75011,114 contain pyroxenes that partly display exsolution lamellae of ~1 μm thickness. Minerals from the brecciated lithology also contain grains with predominantly equilibrated, but also differently zoned specimens. Y-74159 and Y-74450 furthermore show indication for type 5 metamorphism, for example, clouding and augite exsolution lamellae of several μm thickness. This mixture of grains with different degrees of metamorphism let us conclude that mineral fragments of different origins, thermal histories, and postmagmatic overprints were mixed together. Pyroxenes within subophitic lithologies are typically slightly zoned (type 2–3) and/or equilibrated (type 5). Large, clearly zoned pyroxenes from quench-textured lithologies are related to type 1 and thus, represent the least altered lithology among the five analyzed eucrites.

All five eucrites contain regions of glassy areas with a variety of textures similar to proposed impact melts observed in other HED meteorites (Delaney et al. 1984a, 1984b; Mittlefehldt and Lindstrom 1997; Barrat et al. 2011; Mittlefehldt et al. 2013). Investigations of glassy areas in polymict breccias from the HED meteorite clan by Olsen et al. (1990) and Singerling et al. (2013), as well as during this study show petrographic and chemical characteristics, as discussed above, indicating formation of a melt generation during impact events. Considering chemical compositions of optically homogeneous impact melts in HEDs, Barrat et al. (2012) identified two main groups: high Fe/Mg (Fe/Mg $\gg$10) and low Fe/Mg (Fe/Mg < 5). The latter can be subdivided into low-alkali, K-rich (K_2O >0.2 wt%) and Na-rich (Na_2O >0.6 wt%). Compositions of low-alkali-melts are similar to HED bulk rock compositions (Singerling et al. 2013) and therefore, probably formed during large impact events (Schaal et al. 1979; Hörz et al. 2005). Chemical composition of glassy areas from the eucrites analyzed here indicates a relationship to the main group of low Fe/Mg, and to the subgroup of low-alkali melts. The chemical composition of these glasses ranges between pyroxene and plagioclase data (Fig. 8) and could be due

to mixing from both minerals. Thus, we support the idea by Singerling et al. (2013) that low-alkali-melts are melt products of bulk rock material.

In addition to observed widespread thermal metamorphism, formation of secondary Fe-rich olivine veinlets and the Fe-enrichment within pyroxenes might be related to metasomatic activity (Mittlefehldt and Lindstrom 1997; Barrat et al. 2011; Zhang et al. 2013; Warren et al. 2014). These metasomatic reactions are currently debated as an important process on the surface of 4-Vesta, probably provided by a degassing magma ocean (Sarafian et al. 2017). The secondary Fe-rich phases observed in HED meteorites have been analyzed and investigated previously (e.g., Takeda et al. 1983a, 1994a; Warren 2002; Barrat et al. 2011; Roszjar et al. 2011; Zhang et al., 2013; Warren et al. 2014; Mayne et al. 2016; Pang et al. 2017; Patzer and McSween 2018). Barrat et al. (2011) described significant mineralogical changes of unequilibrated eucrites and determined different stages of metasomatism and secondary alteration. According to that work, progressive alteration comprises Fe-enrichment along pyroxene fractures (stage 1); development of fayalitic olivine veinlets (stage 2); and, finally, a development of Al-depleted, Fe-enriched pyroxenes (stage 3). All of these stages are accompanied by the occurrence of accessory phases such as troilite, chromite, and anorthitic plagioclase. Due to the complexity of the analyzed Yamato meteorites, it was not possible to define a distinct secondary alteration stage for each clast according to the scheme proposed by Barrat et al. (2011). All clasts exhibit mineral fragments varying in the observed alteration stage, even in the subophitic texture. Secondary phases such as Fe-enriched pyroxenes and fayalitic olivine veins occur in both chemically zoned and equilibrated pyroxenes in the studied samples. Therefore, the degree of thermal metamorphism of single pyroxene grains seems to be unrelated to the formation or the presence of secondary alteration phases. Secondary phases occur along thermally or mechanically induced cracks within pyroxenes, which indicate a formation after or during brecciation and/or thermal annealing. The occurrence in primary, clearly zoned pyroxenes lacking metamorphic overprint indicate a thermally independent post-magmatic formation process.

Current studies discuss the formation of Fe-rich secondary phases controversially. Here, the influence of a Fe-rich fluid phase under varying temperatures, pressures, and redox conditions (metasomatism; Takeda et al. 1983a; Warren 2002; Barrat et al. 2011; Warren et al. 2014), or a short-term high-temperature process, for example, incongruent melting of pyroxenes, are controlling factors (e.g., Roszjar et al. 2011; Patzer and McSween 2018). Furthermore, several authors described possible alteration features in eucritic clasts in howardites and argued for their origins from evolved crustal melts (Mayne et al. 2016; Hahn et al. 2017). In general, these secondary Fe-rich features within eucrites are still a matter of debate and not the major focus of this work. However, we observe that these Fe-rich veins occur in a variety of pyroxenes metamorphosed to varying degrees, and even within the ones that preserve some igneous zoning. Therefore, this finding supports a late-stage metasomatism scenario. Alternatively, very short-term heating events might have led to incongruent melting and veining leaving the zoning unaffected. For the equilibrated pyroxenes observed in our clasts, no definite answer can be given, but the occurrence of Fe-rich secondary veins within zoned, that is, unmetamorphosed pyroxenes, here strongly favors the metasomatism model, probably triggered by a degassing magma ocean (Sarafian et al. 2017). It is also possible that secondary phases formed during a combination of processes, for example, influence of a fluid phase and a high temperature melting episode. Further work on such Fe enrichments and fayalitic olivines is clearly necessary to disentangle these complex and differing scenarios.

CONCLUSIONS

We have investigated the petrology of five polymict basaltic Yamato eucrites (Y-74159,114, Y-75011,114, Y-793548,66, Y-82210,101, Y-74450,113) containing a variety of lithic clasts with four dominant lithologies including (1) porphyritic, (2) brecciated and partially recrystallized, (3) subophitic, and (4) quench-textured. Despite their variable formation conditions, these lithologies occur within several samples. We therefore suggest that all of these meteorites belong together and derive from closely related parent body source(s) involving at least partially alike source materials in the Vestan crust. Comparison with literature data for these samples is difficult, because textures vary on a local scale, even within thick sections from the same samples. Therefore, we propose that thick sections of respective meteorites, with polymict samples in particular, should be examined carefully before comparison to each other in future studies. We could also show that sample Y-793548 consists of more than one lithic unit and must be classified as a polymict eucrite now instead of a monomict one.

In general, pyroxene compositions of the investigated Yamato samples follow a magmatic chemical trend with Mg-rich cores and Fe-Ca-rich rims, and Ca-rich equilibrated pyroxenes, as typically observed for samples from the HED suite. However, the pyroxene

rim data of the subophitic and especially the quench-textured lithologies T3 and T4 scatter more strongly, and are more Ca-rich compared to pyroxenes derived from the brecciated and porphyritic textures T1 and T2. Equilibrated pyroxenes of the brecciated texture scatter over a wider compositional range compared to data of all other textures, which might be explained by their more diverse origins. Plagioclase fragments within the porphyritic (T1) and brecciated (T2) textures show a larger extent in compositional variation compared to the textures T3 and T4, likely due to the fact that single plagioclase crystals occur as external fragments within the porphyritic texture. Analyzed eucrite samples also contain glassy regions of various textures, and compositional affiliation to the main group of low Fe/Mg, and to the subgroup of low-alkali melts that likely reflect melting of the bulk rock material. Their chemical composition, intermediate to that of the rock-forming silicates, implies a mixing and melting process of previously formed silicates.

Secondary ferroan olivine and Fe-enrichments inside a variety of pyroxene grains are observed in every eucrite clast investigated, forming veins along pre-existing cracks of pyroxenes, and sporadically accompanied by small grains of troilite, chromite, and secondary anorthitic plagioclase. However, the formation of these secondary phases seems to be independent of the degree of thermal metamorphism observed within every type of clast metamorphosed to varying degrees, which would support a late-stage metasomatism model for their formation. All of these observations give important insights into the complex crustal evolution of small differentiated bodies such as 4-Vesta and may aid to interpret spacecraft data on these types of planetary bodies such as the DAWN mission.

Acknowledgments—We thank A. Yamaguchi for the allocation of eucrites samples from the Antarctic meteorite collection at NIPR, the editorial handling and review of the manuscript, an anonymous reviewer for helpful comments, as well as J. Berndt for support with the microprobe analyses. ARS acknowledges support from a NASA Jenkins graduate fellowship (NNX13 AR90H). All authors have no conflict of interest to declare.

Editorial Handling—Dr. Akira Yamaguchi

REFERENCES

Barrat J. A., Yamaguchi A., Greenwood R. C., Bohn M., Cotton J., Benoit M., and Franchi I. A. 2007. The Stannern trend eucrites: Contamination of main group eucritic magmas by crustal partial melts. *Geochimica et Cosmochimica Acta* 71:4108–4124.

Barrat J. A., Yamaguchi A., Bunch T. E., Bohn M., Bollinger C., and Ceuleneer G. 2011. Possible fluid-rock interactions on differentiated asteroids recorded in eucritic meteorites. *Geochimica et Cosmochimica Acta* 75:3839–3852.

Barrat J. A., Bodenan J. D., Yamaguchi A., Buchanan P. C., Toplis M., and Bollinger C. 2012. What can we learn on Vesta from the petrology of impact melts? (abstract #1438). 43rd Lunar and Planetary Science Conference. CD-ROM.

Barrett T. J., Barnes J. J., Tartèse R., Anand M., Franchi I. A., Greenwood R. C., Charlier B. L. A., and Grady M. M. 2016. The abundance and isotopic composition of water in eucrites. *Meteoritics & Planetary Science* 51:1110–1124.

Beck A. W., Welten K. C., McSween H. Y., Viviano C. E., and Caffee M. W. 2012. Petrologic and textural diversity among the PCA 02 howardite group, one of the largest pieces of the Vestan surface. *Meteoritics & Planetary Science* 47:947–969.

Binzel R. P. and Xu S. 1993. Chips off of asteroid 4 Vesta: Evidence for the parent body of basaltic achondrite meteorites. *Science* 260:186–191.

Binzel R. P., Gaffey M. J., Thomas P. C., Zellner B. H., Storrs A. D., and Wells E. N. 1997. Geologic mapping of Vesta from 1994 Hubble Space Telescope images. *Icarus* 128:95–103.

Bobe K. D. 1992. Die monomikten Eukrite und ihre mehrphasige magmatische, impaktmetamorphe und thermische Entwicklungsgeschichte auf dem HED-Mutterkörper. Ph.D. thesis, Universität Münster, Münster, Germany.

Buchanan P. C. and Mittlefehldt D. W. 2003. Lithic components in the paired howardites EET 87503 and EET 87513: Characterization of the regolith of 4 Vesta. *Antarctic Meteorite Research* 16:128–151.

Bunch T. E. 1975. Petrography and petrology of basaltic achondrite polymict breccias (howardites). Proceedings 6th Lunar Science Conference. pp. 469–492.

Consolmagno G. J. and Drake M. J. 1977. Composition and evolution of the eucrite parent body: Evidence from rare earth elements. *Geochimica et Cosmochimica Acta* 41:1271–1282.

De Sanctis M. C., Ammannito E., Capria M. T., Tosi F., Capaccioni F., Zambon F., Carraro F., Fonte S., Frigeri A., Jaumann R., Magni G., Marchi S., McCord T. B., McFadden L. A., McSween H. Y., Mittlefehldt D. W., Nathues A., Palomba E., Pieters C. M., Raymond C. A., Russell C. T., Toplis M. J., and Turrini D. 2012. Spectroscopic characterization of mineralogy and its diversity across Vesta. *Science* 336:697–700.

Delaney J. S., Prinz M., and Takeda H. 1984a. The polymict eucrites. *Journal of Geophysical Research* 89:C251–C288.

Delaney J. S., Prinz M., Nehru C. E., and Stokes C. P. 1984b. Allan Hills A81001 cumulate eucrites and black clasts from polymict eucrites (abstract #1108). 15th Lunar and Planetary Science Conference. pp. 212–213.

Drake M. J. 1979. Geochemical evolution of the eucrite parent body: Possible nature and evolution of asteroid 4 Vesta? In *Asteroids*, edited by Gehrels T. Tucson, Arizona: University of Arizona Press. pp. 765–782.

Drake M. J. 2001. The eucrite/Vesta story. *Meteoritics & Planetary Science* 36:501–513.

Gaffey M. J. 1997. Surface lithologic heterogeneity of asteroid 4 Vesta. *Icarus* 127:130–157.

Graham A. L. and Yanai K. 1986. A review of the Yamato-80,-81 and -82 meteorite collections. *Memoirs of the National Institute of Polar Research Special Issue* 41:167–180.

Haba M. K., Wotzlaw J.-F., Lai Y.-J., Yamaguchi A., and Schönbächler M. 2019. Mesosiderite formation on asteroid 4 Vesta by a hit-and-run collision. *Nature Geoscience* 12:510–515.

Hahn T. M. Jr, Lunning N. G., McSween H. Y. Jr, Bodnar R. J., and Taylor L. A. 2017. Dacite formation on Vesta: Partial melting of the eucritic crust. *Meteoritics & Planetary Science* 52:1173–1196.

Hörz F., Cintala M. J., See T. H., and Loan L. E. 2005. Shock melting of ordinary chondrite powders and implications for asteroidal regoliths. *Meteoritics & Planetary Science* 40:1329–1346.

Keil K., Stöffler D., Love S. G., and Scott E. R. D. 1997. Constraints on the role of impact heating and melting in asteroids. *Meteoritics & Planetary Science* 32:349–363.

Lunning N. G., Welten K. C., McSween H. Y. Jr, Caffee M. W., and Beck A. W. 2016. Grosvenor Mountains 95 howardite pairing group: Insights into the surface of asteroid 4 Vesta. *Meteoritics & Planetary Science* 51:167–194.

Mayne R. G., McSween H. Y. Jr, McCoy T. J., and Gale A. 2009. Petrology of the unbrecciated eucrites. *Geochimica et Cosmochimica Acta* 73:794–819.

Mayne R. G., Smith S. E., and Corrigan C. M. 2016. Hiding in the howardites: Unequilibrated eucrite clasts as a guide to the formation of Vesta's crust. *Meteoritics & Planetary Science* 51:2387–2402.

McCoy T. J., Beck A. W., Prettyman T. H., and Mittlefehldt D. W. 2015. Asteroid 4 Vesta II: Exploring a geologically and geochemically complex world with the DAWN mission. *Chemie der Erde — Geochemistry* 75:273–285.

McSween H. Y. Jr., Mittlefehldt D. W., Beck A. W., Mayne R. G., and McCoy T. J. 2011. HED meteorites and their relationship to the geology of Vesta and the Dawn mission. *Space Science Review* 163:141–174.

Metzler K., Bobe K., Palme H., Spettel B., and Stöffler D. 1995. Thermal and impact metamorphism on the HED parent asteroid. *Planetary and Space Science* 43:499–525.

Mittlefehldt D. W. 2015. Asteroid (4) Vesta: I. The howardite-eucrite-diogenite (HED) clan of meteorites. *Chemie der Erde — Geochemistry* 75:155–183.

Mittlefehldt D. W. and Lindstrom M. M. 1997. Magnesian basalt clasts from the EET 92014 and Kapoeta howardites and a discussion of alleged primary magnesian HED basalts. *Geochimica et Cosmochimica Acta* 61:453–462.

Mittlefehldt D. W., McCoy T. J., Goodrich C. A., and Kracher A. 1998. Non-chondritic meteorites from asteroidal bodies. In *Planetary materials*, edited by Papike J. J. Reviews in Mineralogy, Vol. 36. Washington, D.C.: Mineralogical Society of America.

Mittlefehldt D. W., Herrin J. S., Quinn J. E., Mertzman S. A., Cartwright J. A., Mertzman K. R., and Peng Z. X. 2013. Composition and petrology of HED polymict breccias: The regolith of (4) Vesta. *Meteoritics & Planetary Science* 48:2105–2134.

Miyamoto M., Takeda H., and Yanai K. 1978. Yamato achondrite polymict breccias. *Memoirs of the National Institute of Polar Research, Special Issue* 8:185–197.

Olsen E., Noonan A., Fredriksson K., Jarosewich E., and Moreland G. 1978. Eleven new meteorites from Antarctica, 1976–1977. *Meteoritics* 13:209–225.

Olsen E. J., Fredriksson K., Rajan S., and Noonan A. 1990. Chondrule-like objects and brown glasses in howardites. *Meteoritics* 25:187–194.

Pang R.-L., Zhang A., and Wang R.-C. 2017. Complex origins of silicate veinlets in HED meteorites: A case study of Northwest Africa 1109. *Meteoritics & Planetary Science* 52:2113–2131.

Papike J. J. 1998. Comparative planetary mineralogy: Chemistry of melt-derived pyroxene, feldspar, and olivine. In *Planetary materials*, edited by Papike J. J. Reviews in Mineralogy, vol. 36. Washington, D.C.: Mineralogical Society of America. 7-1–7-11.

Papike J. J., Karner J. M., and Shearer C. K. 2003. Determination of planetary basalt parentage: A simple technique using electron microprobe. *American Mineralogist* 88:469–472.

Patzer A. and McSween H. Y. 2012. Ordinary (mesostasis) and not-so-ordinary (symplectites) late-stage assemblages in howardites. *Meteoritics & Planetary Science* 47:1475–1490.

Patzer A. and McSween H. Y. Jr 2018. Ferroan olivine-bearing eucrite clasts found in howardites. *Meteoritics & Planetary Science* 53:1131–1149.

Pun A. and Papike J. J. 1996. Unequilibrated eucrites and the equilibrated Juvinas eucrite: Pyroxene REE systematic and major, minor, and trace element zoning. *American Mineralogist* 81:1438–1451.

Reid A. M. 1982. Overview of Antarctic achondrites. *Smithsonian Contributions to the Earth Sciences* 24:59–64.

Roszjar J., Metzler K., Bischoff A., Greenwood R. C., and Franchi I. A. 2009. Northwest Africa (NWA) 5073 — A eucritic basalt with cm-sized pyroxenes. *Meteoritics & Planetary Science* 44(Suppl.):A178.

Roszjar J., Metzler K., Bischoff A., Barrat J., Geisler T., Greenwood R. C., Franchi I. A., and Klemme S. 2011. Thermal history of Northwest Africa 5073 — A coarse-grained Stannern-trend eucrite containing cm-sized pyroxenes and large zircon grains. *Meteoritics & Planetary Science* 46:1754–1773.

Roszjar J., Whitehouse M. J., Srinivasan G., Mezger K., Scherer E. E., Van Orman J. A., and Bischoff A. 2016. Prolonged magmatism on 4 Vesta inferred from Hf-W analysis of eucrite zircon. *Earth and Planetary Science Letters* 452:216–226.

Sarafian A. R., John T., Roszjar J., and Whitehouse M. J. 2017. Chlorine and hydrogen degassing in Vesta's magma ocean. *Earth and Planetary Science Letters* 459:311–319.

Schaal R. B., Hörz F., Thompson T. D., and Bauer J. F. 1979. Shock metamorphism of granulated lunar basalt. Proceedings of the 10th Lunar and Planetary Science Conference. pp. 2547–2571.

Schwartz J. M. and McCallum I. S. 2005. Comparative study of equilibrated and unequilibrated eucrites: Subsolidus thermal histories of Haraiya and Pasamonte. *American Mineralogist* 90:1871–1886.

Score R., King T. V., Schwarz A. M., Reid A. M., and Mason B. 1982. Description of stony meteorites. *Smithsonian Contributions to the Earth Sciences* 24:19–48.

Singerling S. A., McSween H. Y. Jr., and Taylor L. A. 2013. Glasses in howardites: Impact melts or pyroclasts? *Meteoritics & Planetary Science* 48:715–729.

Stolper E. 1977. Experimental petrology of eucrite meteorites. *Geochimica et Cosmochimica Acta* 41:587–611.

Takeda H. 1997. Mineralogical records of early planetary processes on the howardite, eucrite, diog-enite parent body with reference to Vesta. *Meteoritics & Planetary Science* 32:841–853.

Takeda H. and Graham A. L. 1991. Degree of equilibration of eucritic pyroxenes and thermal meta-morphism of the earliest planetary crust. *Meteoritics* 26:129–134.

Takeda H. and Yanai K. 1982. Mineralogical examination of the Yamato-79 achondrites: Polymict eucrites and ureilites. *Memoirs of National Institute of Polar Research, Special Issue* 25:97–123.

Takeda H., Miyamoto M., Duke M. B., and Ishii T. 1978. Crystallization of pyroxenes in lunar KREEP basalt 15386 and meteoritic basalts. Proceedings of the 9th Lunar and Planetary Science Conference. pp. 1157–1171.

Takeda H., Wooden J. L., Mori H., Delaney J. S., Prinz M., and Nyquist L. E. 1983a. Comparison of Yamato and Victoria Land polymict eucrites: A view from mineralogical and isotopic studies. Proceedings 14th Lunar and Planetary Science Conference, *Journal of Geophysical Research* 88:B245–B256.

Takeda H., Mori H., Delaney J. S., Prinz M., Harlow G. E., and Ishii T. 1983b. Mineralogical comparison of Antarctic and non-Antarctic HED (howardites-eucrites-diogenites) achondrites. *Memoirs of the National Institute of Polar Research* 30:181–205.

Takeda H., Mori H., and Bogard D. D. 1994. Mineralogy and ^{39}Ar–^{40}Ar age of an old pristine basalt: Thermal history of the HED parent body. *Earth and Planetary Science Letters* 122:183–194.

Warren P. H. 2002. Northwest Africa 1000: A new eucrite with maskelynite, unequilibrated pyroxene crisscrossed by fayalite-rich veins, and Stannern-like geochemistry (abstract #1147). 33th Lunar and Planetary Science Conference. CD-ROM.

Warren P. H., Kallemeyn G. W., and Arai T. 1996. Compositional-petrologic investigation of quench-textured eucrites: Microporphyritic ALH 81001 and vesicular PCA 91007. Lunar and Planetary Institute Technical Report 96-02 Part I. Tucson, Arizona: Lunar and Planetary Institute. pp. 35–37.

Warren P. H., Rubin A. E., Isa J., Gessler N., Ahn I., and Choi B.-G. 2014. Northwest Africa 5738: Multistage fluid-driven secondary alteration in an extraordinarily evolved eucrite. *Geochimica et Cosmochimica Acta* 141: 199–227.

Yamaguchi A. and Takeda H. 1992. Mineralogical study of some brecciated Antarctic eucrites. *Proceedings of the NIPR Symposium on Antarctic Meteorites* 5:242–257.

Yamaguchi A., Taylor G. J., and Keil K. 1996. Global crustal metamorphism of the eucrite parent body. *Icarus* 124:97–112.

Yamaguchi A., Taylor G. J., Keil K., and Bogard D. D. 1997. Evidence for a large cratering event on the HED parent body (Vesta)~4.5 Ga ago. *Meteoritics & Planetary Science* 32:A144.

Yamaguchi A., Taylor G. J., Keil K., Floss C., Crozaz G., Nyquist L. E., Bogard D. D., Garrison D. H., Reese Y. D., Wiesmann H., and Shih C. Y. 2001. Post-crystallization reheating and partial melting of eucrite EET 90020 by impact into the hot crust of asteroid 4-Vesta 4.5 Ga ago. *Geochimica et Cosmochimica Acta* 20:3577–3599.

Yamaguchi A., Barrat J. A., Greenwood R. C., Shirai N., Okamoto C., Setoyanagi T., Ebihara M., Franchi I. A., and Bohn M. 2009. Crustal partial melting on Vesta: Evidence from highly metamorphosed eucrites. *Geochimica et Cosmochimica Acta* 73:7162–7182.

Zhang A. C., Wang R. C., Hsu W. B., and Bartoschewitz R. 2013. Record of S-rich vapors on asteroid 4 Vesta: Sulfurization in the Northwest Africa 2339 eucrite. *Geochimica et Cosmochimica Acta* 109:1–13.

SUPPORTING INFORMATION

Additional supporting information may be found in the online version of this article.

Table S1. Average microprobe analyses in wt% of all pyroxene grains from analyzed textures T1–4.

Table S2. Average microprobe analyses in wt% of all olivine grains and Fe-enriched pyroxene veins from analyzed textures T1–4.

Table S3. Average microprobe analyses in wt% of all plagioclase grains from analyzed textures T1–4.